

Probing universal critical scaling with scan density matrix renormalization group

Chepiga, Natalia

DOI

[10.1103/PhysRevB.110.144401](https://doi.org/10.1103/PhysRevB.110.144401)

Publication date

2024

Document Version

Final published version

Published in

Physical Review B

Citation (APA)

Chepiga, N. (2024). Probing universal critical scaling with scan density matrix renormalization group. *Physical Review B*, 110(14), Article 144401. <https://doi.org/10.1103/PhysRevB.110.144401>

Important note

To cite this publication, please use the final published version (if applicable). Please check the document version above.

Copyright

Other than for strictly personal use, it is not permitted to download, forward or distribute the text or part of it, without the consent of the author(s) and/or copyright holder(s), unless the work is under an open content license such as Creative Commons.

Takedown policy

Please contact us and provide details if you believe this document breaches copyrights. We will remove access to the work immediately and investigate your claim.

Green Open Access added to TU Delft Institutional Repository

'You share, we take care!' - Taverne project

<https://www.openaccess.nl/en/you-share-we-take-care>

Otherwise as indicated in the copyright section: the publisher is the copyright holder of this work and the author uses the Dutch legislation to make this work public.

Probing universal critical scaling with scan density matrix renormalization groupNatalia Chepiga *Kavli Institute of Nanoscience, Delft University of Technology, Lorentzweg 1, 2628 CJ Delft, The Netherlands* (Received 1 July 2024; revised 11 September 2024; accepted 18 September 2024; published 1 October 2024)

We explore the universal signatures of quantum phase transitions that can be extracted with the density matrix renormalization group (DMRG) algorithm applied to quantum chains with a gradient. We present high-quality data collapses for the order parameter and for the entanglement entropy for three minimal models: transverse-field Ising, three-state Potts, and Ashkin-Teller. Furthermore, we show that scan-DMRG successfully captures the universal critical scaling when applied across the magnetic Wess-Zumino-Witten and nonmagnetic Ising transitions in the frustrated Haldane chain. In addition, we report a universal scaling of the lowest excitation energy as a function of a gradient rate. Finally, we argue that the scan-DMRG approach has significantly lower computational cost compare to the conventional DMRG protocols to study quantum phase transitions.

DOI: [10.1103/PhysRevB.110.144401](https://doi.org/10.1103/PhysRevB.110.144401)**I. INTRODUCTION**

Understanding the nature of quantum phase transitions in low-dimensional systems is a central topic of condensed matter physics [1,2]. To a large extent modern theory of phase transitions relies on the concept of universality of the critical scaling insensitive to microscopic details of a particular system. This allows to address quantum phase transitions in real materials with simplified lattice models. Despite their simplicity, these models very rarely can be solved exactly and otherwise require advanced numerical techniques. The density matrix renormalization group (DMRG) algorithm [3–6] is one of the most accurate and widely used numerical tool for quantum chains. The algorithm relies on the area law stating that entanglement of a low-energy state of local Hamiltonians is capped in one dimension (1D). However, at the critical point the area law is violated and the entanglement entropy along with the computational complexity grow with the system size [7]. This makes the usage of either finite- or infinite-size DMRG rather challenging in the context of quantum phase transitions [5,8–12].

In this paper we present an alternative approach to study phase transitions numerically at much lower computational cost using scan-DMRG. In this method an external parameter varies along a chain or a cylinder with a fixed gradient. The scan-DMRG algorithm is traditionally used to probe multiple phases at once—literally, to scan through the phase diagrams [13–16]. It has also been used to qualitatively distinguish magnetic and nonmagnetic domain walls [17]. In this study, focusing on the situation when two gapped phases are connected through a continuous quantum phase transition, we show how the universal signatures of the phase transition can be extracted with scan-DMRG simulations.

Study of quantum chains with linearly varying coupling of field has a long history that roots back to the local density approximation (LDA) [18] that allows to treat the effect of gradients in the system by assuming that the order parameter is locally uniform. However, LDA cannot be applied near critical points where divergent correlation length is inconsistent with locality constraints. Motivated by the nonhomogeneous

trapping potentials in cold atoms experiments, the effect of gradients in Luttinger liquids has been intensely studied with the integrable models and by means of conformal field theory [19–22]. The study of gradients that runs through a single transition point between two gapped phases is mainly limited to the transverse-field Ising and XY chains [23–26]. In this paper, we will show that the nature of isolated quantum critical point can be captured with gradient chains in a generic case.

Typical numerical analysis of quantum phase transitions relies on the critical scaling of three quantities: the order parameter, the energy gap, and the entanglement entropy. In this paper, we will show that in the scan-DMRG all three observables obey the universal scaling. The rest of the paper is organized as follows. In Sec. II, we will present the scan-DMRG results for the three minimal models: Ising, three-state Potts, and Ashkin-Teller describing the transition between the paramagnetic disordered phase and phases with spontaneously broken \mathbb{Z}_2 , \mathbb{Z}_3 and \mathbb{Z}_4 symmetries correspondingly. In Sec. III, we will provide computationally more challenging examples of the Ising and Wess-Zumino-Witten (WZW) [27,28] transitions in a frustrated Haldane chain. In Sec. IV, we will discuss the computational gain of the scan-DMRG algorithm. Finally we summarized our results and bring them into a perspective in Sec. V.

II. SPATIAL KIBBLE-ZUREK MECHANISM IN MINIMAL MODELS**A. Idea**

Interpolation from one phase to another along a chain with a fixed gradient can be viewed as a spatial version of the celebrated Kibble-Zurek mechanism [29–32]. In the original formulation of the mechanism, the system is dynamically driven through a transition and it turns out that the scaling as a function of sweep rate of certain quantities including the number of topological defects (kinks) and the correlation length are universal for a given type of the transition. For a constant sweep rate τ , the characteristic time scale is $t \sim \tau^{v/(1+v)}$ and $\epsilon \sim \frac{t}{\tau} \sim \tau^{\frac{-1}{1+v}}$ is an effective distance to the transition [33].

Here we deal only with conformal transitions and thus set the dynamical critical exponent $z = 1$. By analogy, we define an effective distance to the transition in the gradient chain:

$$x \sim (g - g_c) \delta^{\frac{-1}{1+\nu}} \Rightarrow (g - g_c) \sim x \delta^{\frac{1}{1+\nu}}. \quad (1)$$

Here g is a parameter varying along the chain (on-site transverse field or coupling constant) and g_c mark the location of the transition in the thermodynamic limit, and δ is the gradient rate—the value that shows how much g changes between two consecutive sites or bonds. In this paper we focus on linear gradients, thus when g_i corresponds to the on-site field h_i the gradient is $\delta = \frac{h_N - h_1}{N-1}$. The correlation length diverges upon approaching the transition with the critical exponent ν implying

$$\xi \sim (g - g_c)^{-\nu} \sim x^{-\nu} \delta^{\frac{-\nu}{1+\nu}}. \quad (2)$$

B. Models

Ferromagnetic Ising, three-state Potts and Ashkin-Teller models form an ideal playground to explore quantum phase transitions into \mathbb{Z}_n symmetry breaking phases. In the formulation that we use below, the location of the transitions is known exactly due to the self-duality of the models. Moreover, the operator content and the set of critical exponents are also well established by conformal field theory (CFT) [28].

Let us start with a ferromagnetic transverse field Ising model:

$$H = -J \sum_i S_i^x S_{i+1}^x - \sum_i h_i S_i^z, \quad (3)$$

where $S^{x,z}$ are components of the spin-1/2 operator. We set $J = 1$ and let the transverse field h to interpolate linearly between h_{st} and h_{en} . In the uniform case, the model is critical at $h_c = 0.5$ separating ferromagnetic phase with spontaneously broken spin-flip symmetry for $h < h_c$ and a paramagnet for $h > h_c$. The critical point belongs to the 1+1D Ising universality class and is characterized by the central charge $c = 1/2$, correlation length critical exponent $\nu = 1$ and the order parameter critical exponent $\beta = 1/8$. In the gradient model, we vary a field term h_i .

Ferromagnetic Ising chain defined in the Eq. (3) in terms of spin operators $S^{x,z}$ can alternatively be defined in terms of Pauli matrices $\sigma^{x,z}$:

$$H = -\tilde{J} \sum_i \sigma_i^x \sigma_{i+1}^x - \sum_i \tilde{h}_i \sigma_i^z, \quad (4)$$

in the present case the critical point is located at $\tilde{h}_c = \tilde{J}$.

Secondly, we formulate the ferromagnetic q -state Potts model as a generalization of the Ising model to the case of local Hilbert space $d = q$ defined by the following microscopic Hamiltonian:

$$H_{\text{Potts}} = -J \sum_{i=1}^{N-1} \sum_{\mu=1}^q P_i^\mu P_{i+1}^\mu - \sum_{i=1}^N h_i P_i, \quad (5)$$

where $P_i^\mu = |\mu\rangle_{ii}\langle\mu| - 1/q$ tends to project the spin at site i along the μ direction while $P_i = |\eta_0\rangle_{ii}\langle\eta_0| - 1/q$ tends to align spins along the direction $|\eta_0\rangle_i = \sum_\mu |\mu\rangle / \sqrt{q}$. Without loss of generality, we set $J = 1$ and $h_{\text{st}} \leq h \leq h_{\text{en}}$. This model is identical to the transverse-field Ising model of Eq. 4 when

$q = 2$. The three-state Potts model is realized with $q = 3$. In the uniform case, its critical point is located at $h_c = 1$. The central charge is $c = 4/5$ and critical exponents are $\nu = 5/6$ and $\beta = 1/9$. We introduce gradient through the on-site transverse field term h_i .

Further generalization of Ising and three-state Potts model to the four-dimensional local Hilbert allows an additional freedom. The corresponding minimal model is called the Ashkin-Teller model [34] and is controlled by an asymmetry parameter λ :

$$H = - \sum_i J_i (R_i^1 R_{i+1}^1 + R_i^2 R_{i+1}^2 + \lambda R_i^3 R_{i+1}^3) - h \sum_i M, \quad (6)$$

where the transverse field operator is defined

$$M(\lambda) = \begin{pmatrix} 0 & 1 & 1 & \lambda \\ 1 & 0 & \lambda & 1 \\ 1 & \lambda & 0 & 1 \\ \lambda & 1 & 1 & 0 \end{pmatrix},$$

and R matrices are diagonal with entrees: $R^1 = \text{diag}([1, 1, -1, -1])$; $R^2 = \text{diag}([1, -1, 1, -1])$; $R^3 = \text{diag}([1, -1, -1, 1])$. The parameter λ interpolates between two decoupled Ising chains at $\lambda = 0$ and the fully symmetric four-state Potts point at $\lambda = 1$ that up to a prefactor resembles Eq. (5) with $q = 4$.

There is also an alternative definition of the model in terms of Pauli matrices $\sigma^{x,z}$ and $\tau^{x,z}$:

$$H_{AT} = -h \sum_{j=1}^N (\sigma_j^x + \tau_j^x + \lambda \sigma_j^x \tau_j^x) - \sum_{j=1}^{N-1} J_j (\sigma_j^z \sigma_{j+1}^z + \tau_j^z \tau_{j+1}^z + \lambda \sigma_j^z \tau_j^z \sigma_{j+1}^z \tau_{j+1}^z), \quad (7)$$

Formulated this way, one can easily see that the model is self-dual and in the uniform case its critical point is located at $h = J$ for any value of $0 \leq \lambda \leq 1$.

The Ashkin-Teller universality class is a family of universality classes (also know as a *weak* universality class) with some critical exponents continuously varying as a function of the control parameter λ . For instance, the correlation length critical exponent ν is given by [34,35]

$$\nu = \frac{1}{2 - \frac{\pi}{2} [\text{acos}(-\lambda)]^{-1}}, \quad (8)$$

while the order parameter critical exponent $\beta = \nu/8$. The central charge at the critical point and the scaling dimension $d = \beta/\nu$ are universal for any λ and equal to $c = 1$ and $d = 1/8$ [36] correspondingly. As a main example we will use the Ashkin-Teller model with $\lambda = 0.6$. This corresponds to $\nu \approx 0.7748$ and $\beta \approx 0.0969$. This point is away from special symmetry points Ising ($\lambda = 0$), four-state Potts ($\lambda = 1$), and parafermions ($\lambda = 0.75$) and therefore provides a generic view on the problem.

C. Order parameter

In all three models, we describe the symmetry broken ferromagnetic phase using a local polarization as an order

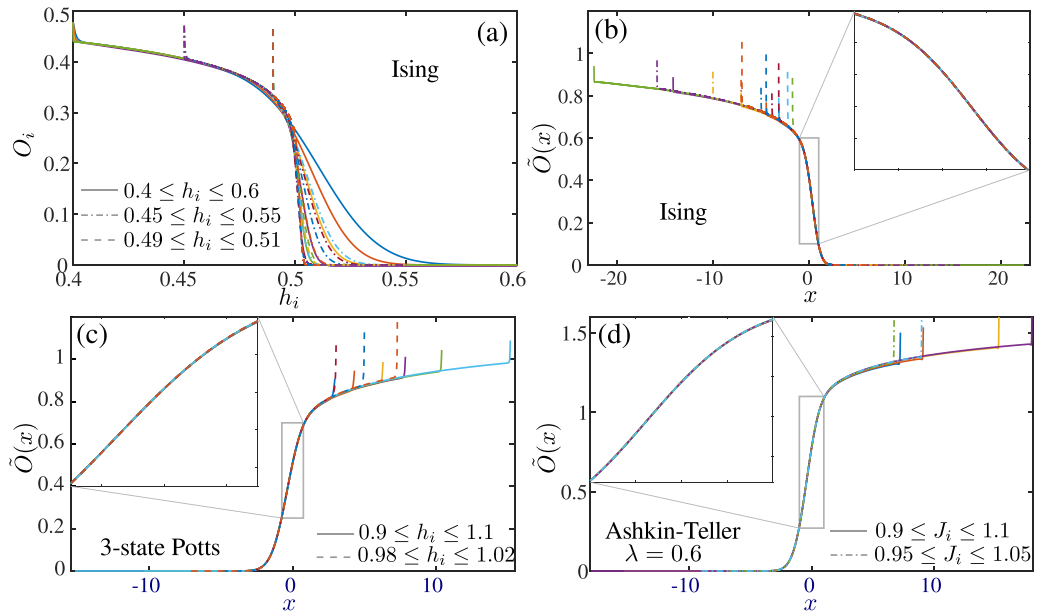


FIG. 1. Local order parameter in quantum chains with a fixed gradient. (a) Raw data for local magnetization as a function of on-site transverse field h_i in the Ising model. (b) Same data rescaled according to Eq. (10): $x = (h_i - h_c)\delta^{-\frac{1}{1+\nu}}$ and $\tilde{O}(x) = O_i\delta^{-\frac{\beta}{1+\nu}}$ with Ising critical exponents $\nu = 1$ and $\beta = 1/8$. [(c) and (d)] Local order parameter rescaled according to Eq. (10) in (c) the gradient three-state Potts chain with $g_i \equiv h_i$, $\beta = 1/9$, and $\nu = 5/6$; and (d) the Ashkin-Teller gradient model with $\lambda = 0.6$, $g_i \equiv J_i$, $\nu \approx 0.7748$, and $\beta \approx 0.0969$. The intervals over which the gradients run are indicated in the legends, different colors correspond to different system sizes ranging between $N = 200$ and $10\,000$ sites for the Ising, between $N = 100$ and $2\,000$ for the Potts, and $N = 400$ and $2\,000$ for the Ashkin-Teller models. For all presented results, we use fixed-free boundary conditions (fixed in the ordered phase). Insets: zoom over indicated areas.

parameter.¹ According to the field theory the order parameter is expected to vanish upon approaching the transition as $O \propto (g - g_c)^\beta$. In Fig. 1(a), we show the raw data for the gradient version of the transverse field Ising model where the left and the right edges of the chain are in the ferromagnetic and paramagnetic phases correspondingly, the critical point is at $h_c = 0.5$. One can see that the gradient δ blurs the power-law decay of the order parameter. The qualitative effect is quite intuitive—the smaller is the gradient step δ the closer is the curve to the continuous field theory prediction. Relying on Eq. (1), we expect

$$O \sim x^\beta \delta^{-\frac{\beta}{1+\nu}}. \quad (9)$$

Similar expression has been obtained for a chain where the gradient runs only through one phase starting with the critical point at one of the edges [37]. Equation (9) implies that upon rescaling the axes to

$$x = (g_i - g_c)\delta^{-\frac{1}{1+\nu}} \quad \text{and} \quad \tilde{O}(x) = O_i\delta^{-\frac{\beta}{1+\nu}}, \quad (10)$$

and $g_i \equiv h_i$, one might expect a perfect data collapse in the critical region. We demonstrate this in Fig. 1(b) where the data presented in (a) are rescaled assuming the Ising critical exponents $\beta = 1/8$ and $\nu = 1$. We use three different windows for the transverse field gradient $|h_i - h_c| \leq 0.01, 0.05, 0.1$ and various system sizes ranging from $N = 200$ to $10\,000$ sites.

¹In order to break the symmetry between the components, we add a boundary field that favors one of the local states at the edge, e.g., $O_i = \langle S_i^z \rangle$ as a local order parameter for the Ising transition with $-h_B S_1^z$ boundary field.

We present similar analysis for the \mathbb{Z}_3 transition in the three-state Potts model defined by Eq. (5). We simulate two windows of the gradient $|h_i - h_c| \leq 0.02, 0.1$ using system sizes between $N = 100$ and $2\,000$. After rescaling the axes according to Eq. (10) with Potts critical exponents $\beta = 1/9$ and $\nu = 5/6$, we obtain a spectacular collapse presented in Fig. 1(c). Magnetization profiles prior to rescaling are provided in the Appendix A.

Finally, in Fig. 1(d), we show the data collapse for the gradient Ashkin-Teller model defined in Eq. (6). Aiming for a generic realization of the Ashkin-Teller transition, we focus on $\lambda = 0.6$ that corresponds to $\nu \approx 0.7748$ and $\beta \approx 0.0969$. In Appendix A, we also provide results prior to the rescaling and for other values of λ . To further stress the universality of our approach in this model, we put a gradient in the ferromagnetic interaction ($g_i \equiv J_i$) while keeping the transverse field uniform. As in the case of Ising and three-state Potts model, the collapse presented in Fig. 1(d) is really spectacular.

D. Energy gap

Relying on the equivalence of the energy and length scales at conformal critical points $\Delta \propto \xi^{-1}$, we get

$$\Delta \sim \delta^{\frac{\nu}{1+\nu}}. \quad (11)$$

This scaling² resembles the form of the energy gap in the Kibble-Zurek mechanism [23]. We compute excitation

²Here we target the lowest excitation energy over the entire chain and thus omit the dependence on x .

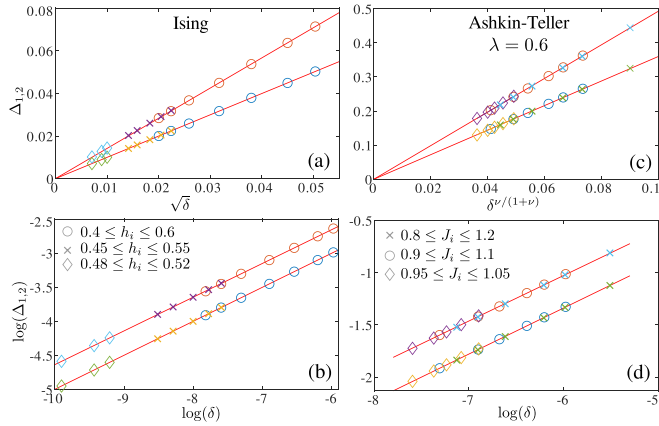


FIG. 2. Scaling of the excitation energy for the two lowest lying excited states in [(a) and (b)] Ising and [(c) and (d)] Ashkin-Teller models as a function of gradient step δ . (a) and (c) present a linear scaling with the inverse of the effective length in agreement with Eq. (11). In (b) and (d), we show excitation energy as a function of a gradient in a log-log scale. Linear fits (red lines) give critical exponents $\nu/(1+\nu) \approx 0.4995$ for the Ising model and ≈ 0.4411 for the Ashkin-Teller one that are in excellent agreement with theory predictions 0.5 and 0.4366 correspondingly. For the Ising model, we present results for systems ranging between $N = 80$ and 800; for the Ashkin-Teller, the range is $80 \leq N \leq 500$. The windows over which the field/coupling runs are indicated in the legends.

energies in a gradient chain by targeting multiple states in DMRG [38].

In Fig. 2, we present the scaling of the excitation energy for two low-lying excited states: in the panels (a) and (b), we

present numerical results for Ising model and in panels (c) and (d), those for the Ashkin-Teller model with $\lambda = 0.6$. The agreement with Eq. (11) is spectacular: performing a linear fit in the log-log scale gives a numerical estimate of the critical exponent $\frac{\nu}{1+\nu}$ agreeing with the theory prediction within 0.1% for the Ising and within 1% for the Ashkin-Teller models.

Interestingly enough, for the Ising model the prefactor A of the lowest excitation $\Delta_1 = A\delta^{\frac{\nu}{1+\nu}}$ is equal to one with a very high precision. This might indicate that *for the lowest excitation* the boundary conditions are approximately equal to polarized at one edge and free at another one, resulting in the conformal tower σ .

E. Entanglement entropy

Entanglement entropy is extracted numerically using the Schmidt values s_α : $S(i) = -\sum_{\alpha=1}^D s_\alpha^2 \ln(s_\alpha^2)$, where i is the site index and the size of the subsystem; D is a bond-dimension that controls the accuracy of DMRG simulations. In the thermodynamic limit the entanglement entropy diverges at the critical point. In scan-DMRG the divergence is bounded by both, the finite-size of the (sub)system as well a finite gradient δ . By either increasing the system size or refining the gradient one approaches the continuum limit. This results in a more pronounced peak as shown in Fig. 3(a) for the Ising model.

According to the study of nonhomogeneous Luttinger liquid [20] the gradient δ produces the logarithmic corrections to the entanglement entropy. We thus define a reduced entanglement entropy as

$$\tilde{S}(x) \sim S(i) + \frac{c}{12} \ln \delta - aC_i, \quad (12)$$

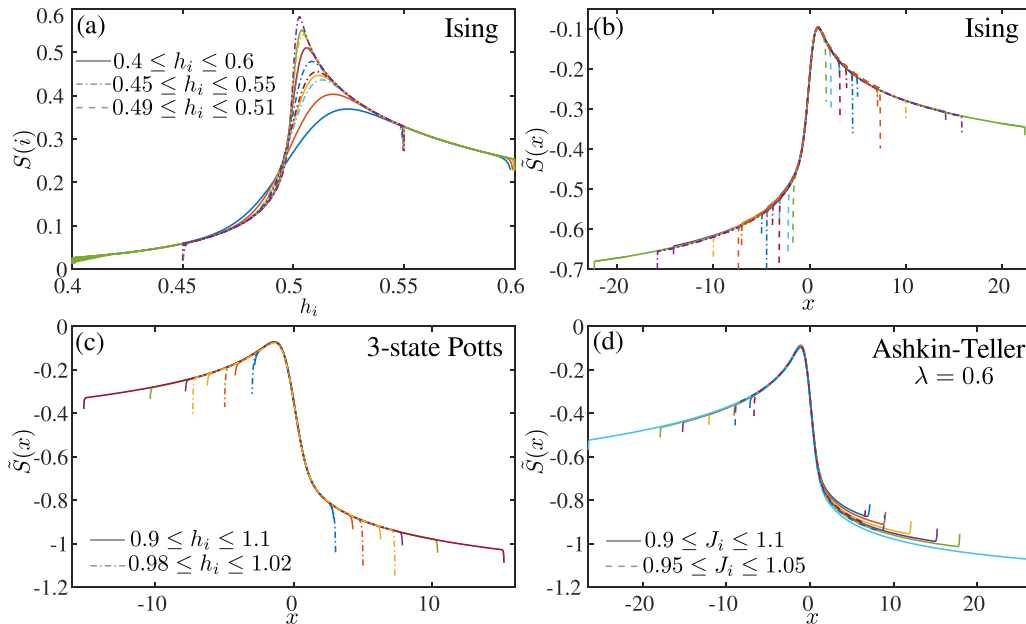


FIG. 3. Entanglement entropy in a gradient chains. (a) Entanglement entropy of the gradient transverse field Ising model. Peak of entanglement entropy approaches the critical point $h_c = 0.5$ upon refining the gradient. (b) Same results rescaled according to Eqs. (12) and (1) with Ising central charge $c = 0.5$ leading to a perfect data collapse in the critical region. [(c) and (d)] Similar data collapse of the entanglement entropy for (c) the three-state Potts transition with $c = 4/5$ and (d) the Ashkin-Teller transition with $c = 1$. The intervals over which the gradients run are indicated in the legends, different colors correspond to different system sizes ranging between $N = 200$ and $N = 10000$ sites for the Ising, between $N = 100$ and 2000 for the Potts, and $N = 400$ and 2000 for the Ashkin-Teller models.

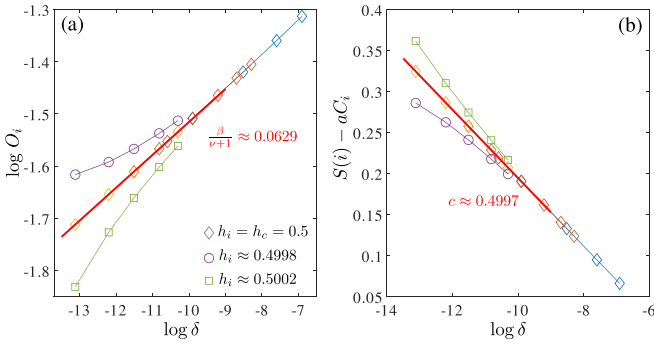


FIG. 4. Extraction of (a) the critical exponent $\frac{\beta}{1+\nu}$, (b) the central charge c . At $h_i = h_c$, the logarithm of the order parameter O_i and the entanglement entropy S_i after removing the Friedel oscillations scale linearly with the logarithm of the gradient rate δ (diamonds, blue, red, and yellow colors state for the gradient ranges $|h_i - h_c| \leq 0.01, 0.05, 0.1$). The slope corresponds to (a) the critical exponent $\beta/(1+\nu)$ and (b) the fraction of the central charge $c/12$. Critical exponent $\frac{\beta}{1+\nu} \approx 0.0629$ extracted numerically by fitting the slope in (a) agrees with the theory prediction for Ising transition $1/16$ within 0.7%. The central charge extracted from the slope in (b) is in excellent agreement with the CFT prediction $c = 1/2$. Away from critical point (circles and squares), the scaling demonstrate a pronounced curvatures, critical point appears as the separatrix in both plots.

where c is the central charge; C_i is a nearest-neighbor correlations. The last term is introduced to remove Friedel oscillations (when applicable) from the entanglement entropy profile [39,40], this is done by optimizing the nonuniversal constant a . The rescaled data as a function of rescaled distance to the transition x are presented in Fig. 12(b) across Ising, (c) across three-state Potts, and (d) across Ashkin-Teller transitions characterized by the central charges $1/2, 4/5$ and 1 correspondingly. Apart from the boundary effect, the collapse looks perfect in the critical region of all models. We believe that small deviation in the ferromagnetic phase of the Ashkin-Teller model in Fig. 3(d) is due to boundary entanglement entropy that comes from the specific fixed boundary conditions that we use. Further progress of boundary field theory in the context of gradient chains are needed to fully clarify and quantify this effect.

F. Numerical extraction of critical exponents and the central charge

The data collapses like those presented in Figs. 1 and 3 provide excellent tests when the underlying universality class can be guessed, for instance, from symmetry arguments. In reality, however, the location of the critical point as well as the exact values of the critical exponents might not be known beforehand. In Figs. 2(b) and 2(d), we have already demonstrated how the critical exponent ν can be extracted from the scaling of the energy gap. In this section, we show how to complete the analysis by extracting the critical exponent β and the central charge c simultaneously identifying the location of the critical point. Let us take the Ising model as an example. From Eqs. (9) and (10), it follows that at the critical point

$h = h_i^3$ the order parameter scales with the gradient rate as $O_i \propto \delta^{\frac{\beta}{1+\nu}}$. It implies that at the critical point the scaling will be linear in the log-log scale while the slope would give $\frac{\beta}{1+\nu}$. A typical scaling is presented with diamonds in Fig. 4(a) where different colors corresponds to different start and end points. Important, that away from the critical point the scaling is not linear but concave in the disordered phase and convex in the ordered one. The critical point is thus appears as a separatrix ensuring a highly accurate location of the critical point. By combining these results with previously critical exponent ν extracted from the scaling of the energy gap, one can calculate the critical exponent β .

In addition, the entanglement entropy (after removing the Friedel oscillations) at $h = h_i$ scales linearly with the $\ln \delta$ with the prefactor proportional to the central charge according to Eq. (12). An example presented in Fig. 4(b) demonstrates an excellent accuracy in the numerically extracted value of the central charge. Again, the critical point appears as a separatrix providing an alternative route to locate the transition.

III. SCAN-DMRG FOR THE FRUSTRATED HALDANE CHAIN

In this section, we will demonstrate the robustness of the presented scan-DMRG approach beyond the simplest minimal models. As an example we consider dimerization transitions in the frustrated Haldane chain: (1) nonmagnetic Ising transition and (2) magnetic Wess-Zumino-Witten (WZW) $SU(2)_2$ transition. Both have been realized in the spin-1 chain with bilinear-biquadratic interaction [41–43] and in the J_1 - J_2 - J_3 model [8] that we will use here and for which the location of the critical points is known with a good accuracy. The J_1 - J_2 - J_3 model is defined by the following microscopic Hamiltonian:

$$H = J_1 \sum_i \mathbf{S}_i \cdot \mathbf{S}_{i+1} + J_2 \sum_i \mathbf{S}_i \cdot \mathbf{S}_{i+2} + \sum_i J_{3i} [(\mathbf{S}_i \cdot \mathbf{S}_{i+1})(\mathbf{S}_{i+1} \cdot \mathbf{S}_{i+2}) + \text{H.c.}], \quad (13)$$

where the first two terms describe Heisenberg interactions on nearest- and next-nearest-neighbors; J_3 term appears in the next-to-leading order expansion of the two-band Hubbard model and known to produce the dimerized phase with spontaneously broken translation symmetry and a twofold degenerate ground state [44]. Here we set $J_1 = 1$.

As a local order parameter, we use the dimerization $O(i) = |\mathbf{S}_i \cdot \mathbf{S}_{i+1} - \mathbf{S}_{i+1} \cdot \mathbf{S}_{i+2}|$ that we further rescale following Eq. (10). For the Ising transition that takes place at $J_2 \approx 0.7$ and $J_3 \approx 0.058$ [8], we observe a perfect collapse of the order parameter in Fig. 5(a); edge effects are noticeably stronger in the disordered - next-nearest-neighbor Haldane - phase than those that we have observe in the Ising model in Fig. 1(b). Collapse of the entanglement entropy presented in Fig. 5(c) is very good in the critical region close to $x = 0$, but we also see a systematic deviation in the disordered phase. Similar to the results of the Ashkin-Teller model we believe

³In the rescaled version $h = h_i$ corresponds to $x = 0$, but here one does not have to perform the rescaling.

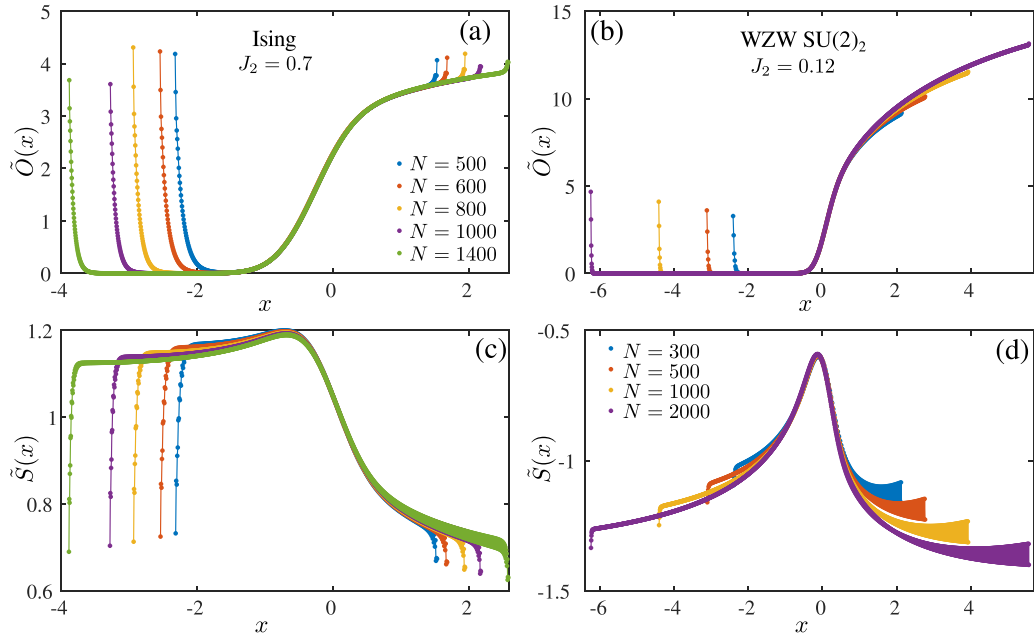


FIG. 5. Scaling of [(a) and (b)] the order parameter and [(c) and (d)] the entanglement entropy across [(a) and (c)] nonmagnetic Ising transition and [(b) and (d)] the Wess-Zumino-Witten transition in the frustrated spin-1 chain. The linear gradient is applied to the J_3 coupling such that [(a) and (c)] at the left edge $J_3 = 0.04$ and at the right one $J_3 = 0.07$; [(b) and (d)] at the left edge $J_3 = 0.05$ and at the right one $J_3 = 0.12$. For both transitions, we see an extremely accurate collapse of the order parameter—the dimerization $O(i) = |\mathbf{S}_i \cdot \mathbf{S}_{i+1} - \mathbf{S}_{i+1} \cdot \mathbf{S}_{i+2}|$. All results are performed with free boundary conditions.

that there might be an additional contribution due to a specific boundary conditions in the next-nearest-neighbor Haldane phase. In the Appendix B we also present these results prior to the rescaling.

To explore the spatial Kibble-Zurek mechanism across the WZW transition we run a gradient through the critical point $J_2 \approx 0.12$, $J_3 \approx 0.087$ where logarithmic corrections vanish [8]. After the rescaling the order parameter shows a spectacular collapse with some minor edge effects in the dimerized phase [see Fig. 5(b)]. Entanglement entropy presented in Fig. 5(d) is collapsed in the vicinity of the transitions, though it shows a strong finite-size effects in the domains of the gapped phases far from the critical region. The nonrescaled data as well as the results for the WZW transition in the presence of the logarithmic corrections are reasonably good and are presented in Appendix B.

With the scan-DMRG one can also very naturally identify the nature of domain walls. For instance, the domain wall between topologically nontrivial Haldane phase and topologically trivial dimerized one hosts a spinon [45,46]. This spinon at the boundary of two domains is clearly visible in the local magnetization profile across the WZW transition presented in Fig. 6. By contrast, numerically extracted local magnetization in the gradient spin-1 chain crossing a nonmagnetic Ising transition at $J_2 = 0.7$ never exceeds 10^{-10} .

IV. COMPUTATIONAL GAIN

The main advantage of the scan-DMRG technique in the context of quantum criticality is its significantly lower computational cost. Intuitively, this is very natural—the chain almost entirely is inside one of the two gapped phases that obey the

area law. Although the area law is violated in the critical region and the entanglement grows it is still capped by the gradient due to spatial Kibble-Zurek mechanism. Let us now quantify possible computational advantage. In the DMRG the entanglement entropy is directly related to the bond dimension $D \propto \exp(S)$, while the leading computational complexity scales as D^3 . In Fig. 7, we present the bond dimension needed to keep all singular values exceeding 10^{-8} for a given system size of (a) $N = 100$ and (b) 400 and for a variety of couplings that range around its critical value for the Ashkin-Teller point with $\lambda = 0.6$. For a uniform system without a gradient [light

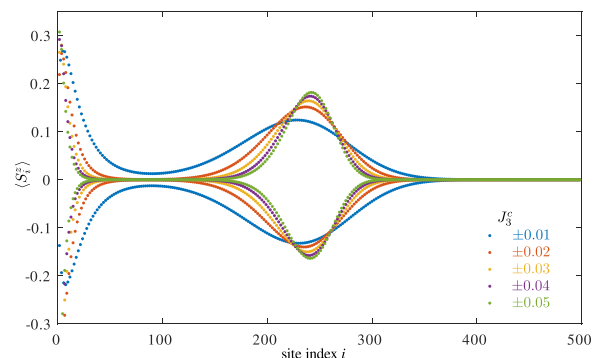


FIG. 6. Appearance of spinons at the edges of the domain of topologically nontrivial Haldane phase in scan-DMRG that runs through the WZW transition in J_1 - J_2 - J_3 model with $J_2 = 0.12$. Legend specifies the window of the J_3 coupling. These results were obtained with $N = 500$. One spin-1/2 is localized at the left edge of the chain. The second spin-1/2 appears as a magnetic domain wall between the Haldane and the dimerized phases.

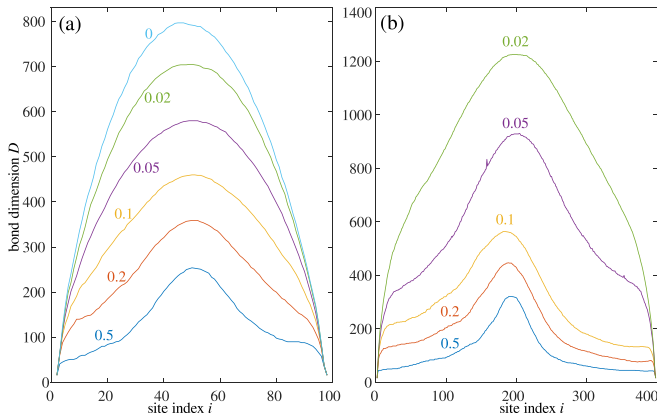


FIG. 7. Bond dimension along a finite size chain with (a) $N = 100$ and (b) 400 sites for the Ashkin-Teller model with $\lambda = 0.6$ and with gradient in the coupling around its critical point $J_c = 1$. The range of the gradient is indicated for each curve, 0 means uniform case without gradient. We choose asymmetric free-fixed boundary conditions necessary to extract the order parameter with local operators. One can see that the bond dimension and associated complexity of the scan-DMRG that scales as D^3 is significantly reduced with the gradient window. Presented bond dimension reflects the number of singular values above 10^{-8} .

blue curve in Fig. 7(a)], the entanglement along with the bond dimension D are the largest. Slight asymmetry in the dome comes from the asymmetric free-fixed boundary conditions that for consistency, we keep the same as for the gradient case. One can see that gradient ranging within $J_i - J_c \in [-0.1, 0.1]$ reduces the maximal bond dimension by a factor of ≈ 2 , and thus the complexity is reduced by a factor of 8. Computational gain is even larger for longer chains.

For the frustrated Haldane chain and WZW transition the computational advantage of scan-DMRG is even more evident. In Fig. 8, we present the DMRG bond dimension required to keep all singular values above 10^{-6} . One can

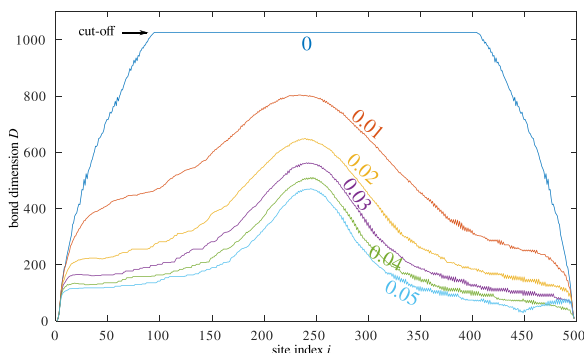


FIG. 8. Bond dimension along a finite size chain with $N = 500$ for the J_1 - J_2 - J_3 model with $J_2 = 0.12$ and with gradient in three-site coupling J_3 around its critical point $J_3^c \approx 0.087$. The range of the gradient is indicated for each curve: 0.05 means the range $0.037 \leq J_{3i} \leq 0.127$; 0 means uniform case without a gradient. Presented bond dimension reflects the number of singular values above 10^{-6} ; for the uniform case, we cannot keep sufficient number of states and cut the bond dimension at $D_{\max} = 1027$.

immediately see that in the uniform case, the bond dimension grows so fast and actually exceeds our cut-off $D_{\max} \approx 10^3$. By contrast, for the gradient that deviates only by ∓ 0.01 from the transition, the bond dimension hardly reaches $D \approx 800$. In Figs. 5(b) and 5(d), we present a scan-DMRG results for the gradient with an approximate range ± 0.035 .

V. SUMMARY AND OUTLOOK

In this paper, we have introduced the scan-DMRG algorithm as a numerical tool to investigate universal signatures of quantum phase transitions. We have provided convincing evidence of the universal scaling of the order parameter, excitation energy, and entanglement entropy across various continuous transitions between gapped phases in quantum chains. We benchmarked our method with three paradigmatic examples of conformal field theory and quantum many-body lattice models: Ising, three-state Potts, and Ashkin-Teller. Furthermore, we have demonstrated the robustness of the spatial Kibble-Zurek mechanism as a tool to probe quantum phase transitions by applying it to the dimerization transitions in the frustrated Haldane chain. We have shown that a convincing data collapse can be produced even when the location of the critical point is not exact; the interval of the gradient is not centered around the critical point; the translation symmetry broken in one of the phases induces strong Friedel oscillations of the entanglement entropy.

The main advantage of scan-DMRG as a tool to study quantum phase transitions is the significantly reduced computational cost. Compare to the techniques based on the scaling at the quantum critical points, including, for instance, extraction of the central charge with finite-size entanglement scaling, the scan-DMRG method allow to reduce the computational cost by an order of magnitude. The scan-DMRG also provides a systematic access to the exponents β and ν describing the critical scaling away from the transition. Although with the uniform DMRG algorithm the convergence away from the criticality is typically not an issue, the process of fitting the numerical data in order to extract critical exponents is usually associated with compromises between taking enough points within the critical region (i.e., not too far from the transition) yet to have correlation length and boundary effects sufficiently small compare to the available system sizes (i.e., also not too close to the transition). Typically this requires a dozens of data points on each side of the transition. Scan-DMRG allows an elegant solution to the problem giving a simultaneous access to both sides of the transition, while the quality of the collapse can be assessed even with a very few samples.

Although scan-DMRG appears as a ready-to-use technique for many practical applications, in this work we limit ourselves to the simplest scenario of a direct continuous transition between two gapped phases. This naturally poses the number of relevant questions that are left for future exploration. How and whether scan-DMRG algorithm can be used for the cases when transition goes through a two-step process with a (possibly narrow) intermediate phase and two distinct transitions? Whether scan-DMRG is suitable to probe continuous transitions where the relevant order parameter is nonlocal, including, in particular, the commensurate-incommensurate

transitions. Whether scan-DMRG is suitable to distinguish between continuous and first-order transitions [47]. Could scan-DMRG capture the transition when at least one phase is critical, the paradigmatic example could be the Kosterlitz-Thouless transition [48]? And if yes, whether there still will be a reasonable advantage in the computational costs? We hope that this study will further stimulate analytical and numerical investigation of gradient quantum systems and their applications in the context of cold atom experiments.

ACKNOWLEDGMENTS

I thank T. Giamarchi and J. Soto Garcia for insightful discussions. This research has been supported by Delft Technology Fellowship. Numerical simulations have been performed at the DelftBlue HPC and at the Dutch national e-infrastructure with the support of the SURF Cooperative.

APPENDIX A: ADDITIONAL DATA FOR GRADIENT POTTS AND ASHKIN-TELLER MODELS

In this section, we provide some additional data for the three-state Potts and Ashkin-Teller models. Firstly, in Fig. 9, we present local magnetization profiles without rescaling as a function of local field h_i [in Fig. 9(a)] [or a coupling J_i [in Fig. 9(b)]. The corresponding data collapses are presented in Figs. 1(c) and 1(d).

Secondly, we present the nonrescaled data for the entanglement entropy in the gradient three-state Potts and

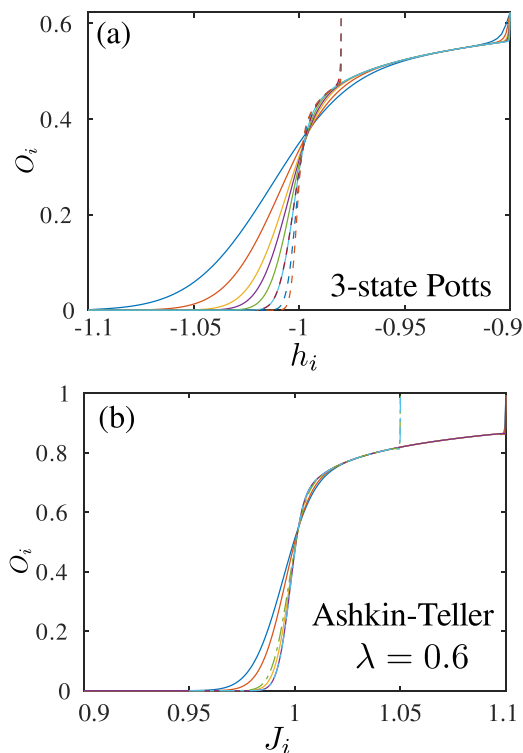


FIG. 9. Local magnetization of (a) the in-homogeneous three-state Potts with linear gradient in the transverse field and (b) the in-homogeneous Ashkin-Teller model with $\lambda = 0.6$ and linear gradient in the couplings constant. As presented in Figs. 1(c) and 1(d) after rescaling these sets of data demonstrate spectacular collapses.

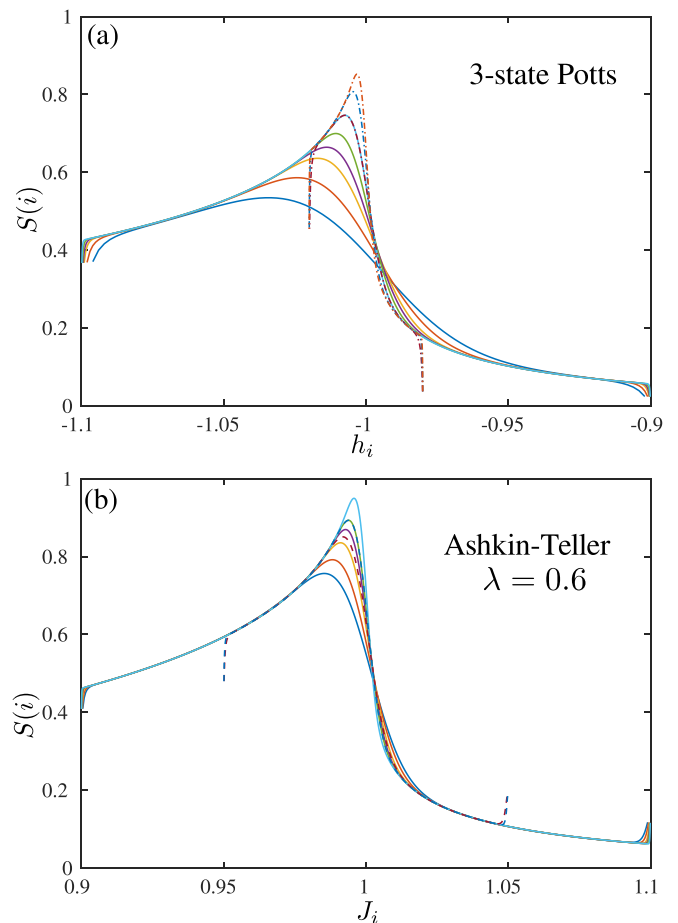


FIG. 10. Entanglement entropy of (a) the in-homogeneous three-state Potts with linear gradient in the transverse field and (b) the in-homogeneous Ashkin-Teller model with $\lambda = 0.6$ and linear gradient in the couplings constant. Peak of entanglement entropy approaches the critical points upon refining the gradient. The rescaled data are presented in Figs. 3(c) and 3(d).

Ashkin-Teller models in Fig. 10. The rescaled data are presented in Figs. 3(c) and 3(d). In both cases, the peak of entanglement grows with $1/\delta$. For three-state Potts model, the gradient runs within the window $|h_i - h_c| < 0.02$ (dash-dotted line) and $|h_i - h_c| < 0.1$ (solid lines). We perform simulations on chains with the lengths ranging from 100 and up to 2000 sites. For the Ashkin-Teller model the two parameter windows we use are $|J_i - J_c| < 0.05$ and 0.1 and system sizes ranging between 400 and 2000 sites.

We also present a systematic study of the collapse of the order parameter and the entanglement entropy for various values of λ to ensure that our analysis is generic and valid for any critical point of the Ashkin-Teller weak universality class. These results are summarized in Fig. 11, where in addition to the results for $\lambda = 0.6$ presented in the main text, we also show the results for $\lambda = 0.2, 0.8$, and 1. The results for the four-state Potts point at $\lambda = 1$ are of special interest because at this point, the critical Ashkin-Teller theory has logarithmic corrections. From the collapses presented in Figs. 11(f) and 11(i), we see that for accessible system sizes the effect of these corrections is not visible and the collapses are still very clean.

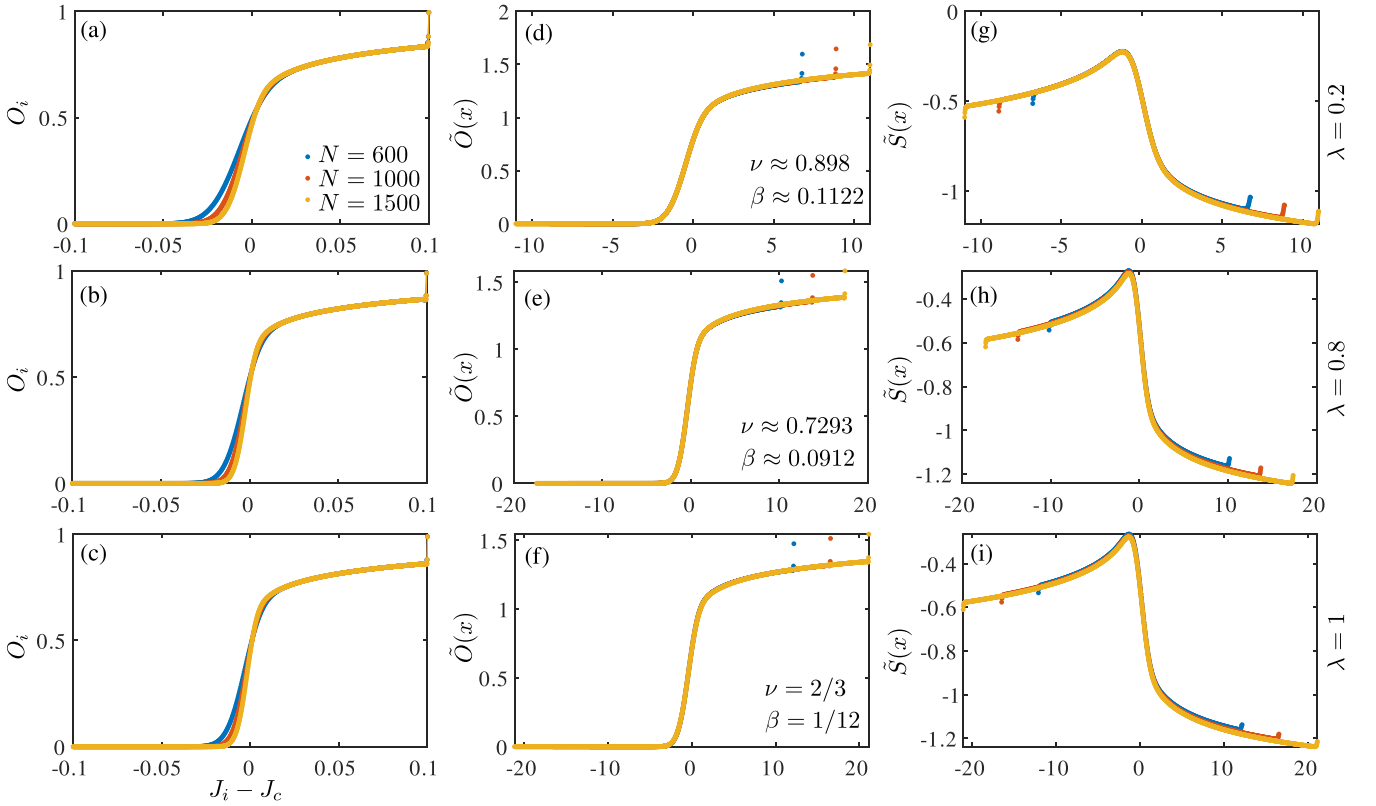


FIG. 11. Data collapse for various Ashkin-Teller transitions with (top) $\lambda = 0.2$, (middle) $\lambda = 0.8$, and (bottom) $\lambda = 1$ (the four-state Potts). [(a)–(c)] Nonrescaled local order parameter O_i as a function of distance to the critical Ashkin-Teller point $J_c = 1$; [(d)–(f)] same data rescaled according to Eq. (10) with indicated critical exponents. [(g)–(i)] Collapse of the rescaled entanglement entropy.

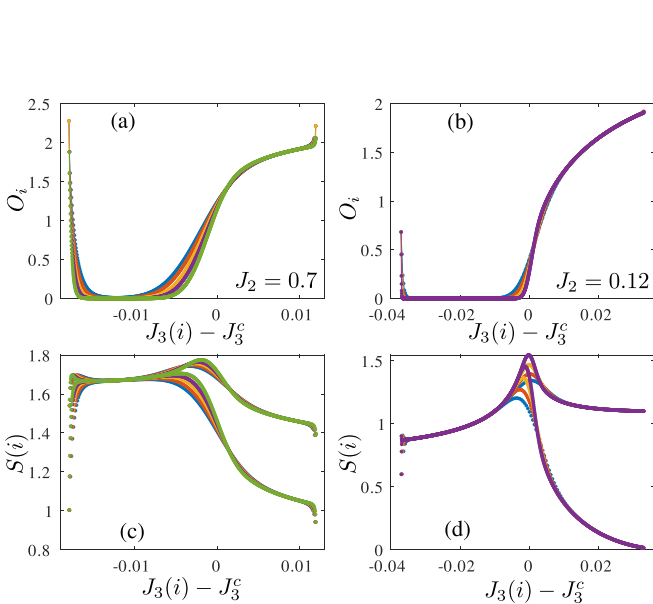


FIG. 12. Nonrescaled [(a) and (b)] dimerization and [(c) and (d)] entanglement entropy across [(a) and (c)] Ising and [(b) and (d)] WZW transitions in spin-1 J_1 - J_2 - J_3 chain [8]. There are strong oscillations in entanglement entropy in the dimerized phase due to broken translation symmetry. [(a) and (c)] For the Ising transition the system sizes range from 500 (blue) to 1400 (green). [(b) and (d)] For the WZW transition we show results between $N = 300$ (blue) and 2000 (purple). The rescaled data are presented in the Fig. 5 of the main text.

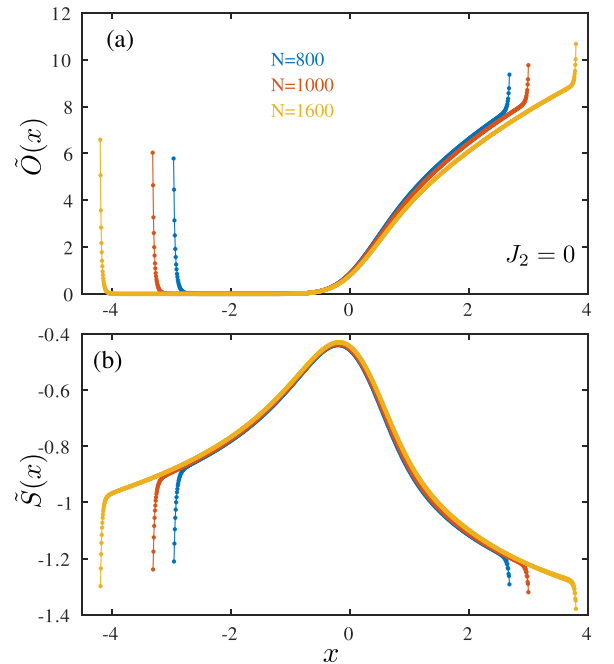


FIG. 13. Rescaled (a) local dimerization and (b) entanglement entropy as a function of the rescaled three-site coupling constant J_{3i} of J_1 - J_2 - J_3 model with $J_1 = 1$ and $J_2 = 0$. The start and end points are fixed to $J_{3,\text{st}} = 0.09$ and $J_{3,\text{en}} = 0.13$; the critical point is located at $J_3^c \approx 0.111$ [44]. At this point, the transition is expected to be in WZW $SU(2)_2$ universality class with some logarithmic corrections.

APPENDIX B: ADDITIONAL DATA FOR FRUSTRATED SPIN-1 CHAIN

In the Fig. 5 of the main text, we presented a data collapse for the Ising and WZW transitions in the J_1 - J_2 - J_3 model. The nonrescaled data are presented in Fig. 12. One can see, in particular, large oscillations of the entanglement entropy in the dimerized phase.

In the main text, we probe a special end point of the WZW critical line located at $J_2 \approx 0.12$ and $J_3 \approx 0.087$; at this point, logarithmic corrections generically present in the critical theory due to marginal operator vanish. Here we also present

the data collapse for $J_2 = 0$ where the logarithmic corrections are present. We can see that for the entanglement entropy the collapse is still spectacular. For the order parameter, we see significant deviations. This is not surprising: the measured effective scaling dimension at $J_2 = 0$ is $d_{\text{eff}} \approx 0.43$ almost 15% larger than the field theory prediction $d = 3/8$ and the value extracted at the end point [8]. If we allow the critical exponents in the rescaling functions of Eq. (10) to deviate within 15% from the CFT values, we again recover a perfect collapse as shown in Fig. 13. Further detailed field-theory analysis is needed to incorporate logarithmic corrections into gradient spin chains.

-
- [1] T. Giamarchi, *Quantum Physics in One Dimension*, International Series of Monographs on Physics (Clarendon Press, Oxford, 2004).
- [2] A. M. Tsvelik, *Quantum Field Theory in Condensed Matter Physics*, 2nd ed. (Cambridge University Press, Cambridge, UK, 2023).
- [3] S. Östlund and S. Rommer, Thermodynamic limit of density matrix renormalization, *Phys. Rev. Lett.* **75**, 3537 (1995).
- [4] U. Schollwöck, The density-matrix renormalization group, *Rev. Mod. Phys.* **77**, 259 (2005).
- [5] U. Schollwöck, The density-matrix renormalization group in the age of matrix product states, *Ann. Phys.* **326**, 96 (2011).
- [6] S. R. White, Density matrix formulation for quantum renormalization groups, *Phys. Rev. Lett.* **69**, 2863 (1992).
- [7] P. Calabrese and J. Cardy, Entanglement entropy and conformal field theory, *J. Phys. A: Math. Theor.* **42**, 504005 (2009).
- [8] N. Chepiga, I. Affleck, and F. Mila, Dimerization transitions in spin-1 chains, *Phys. Rev. B* **93**, 241108(R) (2016).
- [9] N. Chepiga and F. Mila, Lifshitz point at commensurate melting of chains of Rydberg atoms, *Phys. Rev. Res.* **3**, 023049 (2021).
- [10] A. A. Eberharter, L. Vanderstraeten, F. Verstraete, and A. M. Läuchli, Extracting the speed of light from matrix product states, *Phys. Rev. Lett.* **131**, 226502 (2023).
- [11] R.-Z. Huang, L. Zhang, A. M. Läuchli, J. Haegeman, F. Verstraete, and L. Vanderstraeten, Emergent conformal boundaries from finite-entanglement scaling in matrix product states, *Phys. Rev. Lett.* **132**, 086503 (2024).
- [12] M. Yang, B. Vanhecke, and N. Schuch, Detecting emergent continuous symmetries at quantum criticality, *Phys. Rev. Lett.* **131**, 036505 (2023).
- [13] S. Jiang, J. Romhányi, S. R. White, M. E. Zhitomirsky, and A. L. Chernyshev, Where is the quantum spin nematic? *Phys. Rev. Lett.* **130**, 116701 (2023).
- [14] S. Jiang, D. J. Scalapino, and S. R. White, Pairing properties of the $t-t'-t''-j$ model, *Phys. Rev. B* **106**, 174507 (2022).
- [15] S. Jiang and S. R. White, and A. L. Chernyshev, Quantum phases in the honeycomb-lattice J_1 - J_3 ferro-antiferromagnetic model, *Phys. Rev. B* **108**, L180406 (2023).
- [16] Z. Zhu, P. A. Maksimov, S. R. White, and A. L. Chernyshev, Topography of spin liquids on a triangular lattice, *Phys. Rev. Lett.* **120**, 207203 (2018).
- [17] N. Chepiga and F. Mila, Dimerization and effective decoupling in two spin-1 generalizations of the spin- $\frac{1}{2}$ majumdar-ghosh chain, *Phys. Rev. B* **100**, 104426 (2019).
- [18] W. Kohn and L. J. Sham, Self-consistent equations including exchange and correlation effects, *Phys. Rev.* **140**, A1133 (1965).
- [19] A. Bastianello, J. Dubail, and J.-M. Stéphan, Entanglement entropies of inhomogeneous Luttinger liquids, *J. Phys. A: Math. Theor.* **53**, 155001 (2020).
- [20] J. Dubail, J.-M. Stéphan, J. Viti, and P. Calabrese, Conformal field theory for inhomogeneous one-dimensional quantum systems: the example of non-interacting Fermi gases, *SciPost Phys.* **2**, 002 (2017).
- [21] V. Eisler and D. Bauernfeind, Front dynamics and entanglement in the XXZ chain with a gradient, *Phys. Rev. B* **96**, 174301 (2017).
- [22] T. Hikihara and T. Nishino, Connecting distant ends of one-dimensional critical systems by a sine-square deformation, *Phys. Rev. B* **83**, 060414(R) (2011).
- [23] J. Dziarmaga, Dynamics of a quantum phase transition and relaxation to a steady state, *Adv. Phys.* **59**, 1063 (2010).
- [24] J. Dziarmaga and M. M. Rams, Adiabatic dynamics of an inhomogeneous quantum phase transition: the case of a $z > 1$ dynamical exponent, *New J. Phys.* **12**, 103002 (2010).
- [25] A. Niederberger, M. M. Rams, J. Dziarmaga, F. M. Cucchiatti, J. Wehr, and M. Lewenstein, Disorder-induced order in quantum XY chains, *Phys. Rev. A* **82**, 013630 (2010).
- [26] W. H. Zurek and U. Dörner, Phase transition in space: how far does a symmetry bend before it breaks? *Philos. Trans. R. Soc. London, Ser. A* **366**, 2953 (2008).
- [27] I. Affleck, D. Gepner, H. J. Schulz, and T. Ziman, Critical behaviour of spin- s Heisenberg antiferromagnetic chains: analytic and numerical results, *J. Phys. A: Math. Gen.* **22**, 511 (1989).
- [28] P. Di Francesco, P. Mathieu, and D. Sénéchal, *Conformal Field Theory*, Graduate Texts in Contemporary Physics (Springer, New York, 1997).
- [29] J. Dziarmaga, Dynamics of a quantum phase transition: Exact solution of the quantum Ising model, *Phys. Rev. Lett.* **95**, 245701 (2005).
- [30] A. Keesling, A. Omran, H. Levine, H. Bernien, H. Pichler, S. Choi, R. Samajdar, S. Schwartz, P. Silvi, S. Sachdev, P. Zoller, M. Endres, M. Greiner, V. Vuletić, and M. D. Lukin, Quantum Kibble-Zurek mechanism and critical dynamics on a programmable Rydberg simulator, *Nature (London)* **568**, 207 (2019).

- [31] A. Polkovnikov, Universal adiabatic dynamics in the vicinity of a quantum critical point, *Phys. Rev. B* **72**, 161201(R) (2005).
- [32] W. H. Zurek, U. Dorner, and P. Zoller, Dynamics of a quantum phase transition, *Phys. Rev. Lett.* **95**, 105701 (2005).
- [33] A. Francuz, J. Dziarmaga, B. Gardas, and W. H. Zurek, Space and time renormalization in phase transition dynamics, *Phys. Rev. B* **93**, 075134 (2016).
- [34] M. Kohmoto, M. den Nijs, and L. P. Kadanoff, Hamiltonian studies of the $d = 2$ Ashkin-Teller model, *Phys. Rev. B* **24**, 5229 (1981).
- [35] A. O'Brien, S. D. Bartlett, A. C. Doherty, and S. T. Flammia, Symmetry-respecting real-space renormalization for the quantum Ashkin-Teller model, *Phys. Rev. E* **92**, 042163 (2015).
- [36] J. C. Bridgeman, A. O'Brien, S. D. Bartlett, and A. C. Doherty, Multiscale entanglement renormalization ansatz for spin chains with continuously varying criticality, *Phys. Rev. B* **91**, 165129 (2015).
- [37] M. Collura, D. Karevski, and L. Turban, Gradient critical phenomena in the Ising quantum chain: surface behaviour, *J. Stat. Mech.: Theory Exp.* (2009) P08007.
- [38] N. Chepiga and F. Mila, Excitation spectrum and density matrix renormalization group iterations, *Phys. Rev. B* **96**, 054425 (2017).
- [39] S. Capponi, P. Lecheminant, and M. Moliner, Quantum phase transitions in multileg spin ladders with ring exchange, *Phys. Rev. B* **88**, 075132 (2013).
- [40] N. Laflorencie, E. S. Sørensen, M.-S. Chang, and I. Affleck, Boundary effects in the critical scaling of entanglement entropy in 1D systems, *Phys. Rev. Lett.* **96**, 100603 (2006).
- [41] L. A. Takhtajan, The picture of low-lying excitations in the isotropic Heisenberg chain of arbitrary spins, *Phys. Lett. A* **87**, 479 (1982).
- [42] H. M. Babujian, Exact solution of the isotropic Heisenberg chain with arbitrary spins: Thermodynamics of the model, *Nucl. Phys. B* **215**, 317 (1983).
- [43] N. Chepiga, I. Affleck, and F. Mila, Comment on "frustration and multicriticality in the antiferromagnetic spin-1 chain", *Phys. Rev. B* **94**, 136401 (2016).
- [44] F. Michaud, F. M. C. Vernay, S. R. Manmana, and F. Mila, Antiferromagnetic spin- S chains with exactly dimerized ground states, *Phys. Rev. Lett.* **108**, 127202 (2012).
- [45] N. Chepiga, I. Affleck, and F. Mila, Spontaneous dimerization, critical lines, and short-range correlations in a frustrated spin-1 chain, *Phys. Rev. B* **94**, 205112 (United Kingdom, 2016).
- [46] L. Vanderstraeten, E. Wybo, N. Chepiga, F. Verstraete, and F. Mila, Spinon confinement and deconfinement in spin-1 chains, *Phys. Rev. B* **101**, 115138 (2020).
- [47] J. D'Emidio, A. A. Eberharther, and A. M. Läuchli, Diagnosing weakly first-order phase transitions by coupling to order parameters, *SciPost Phys.* **15**, 061 (2023).
- [48] J. M. Kosterlitz and D. J. Thouless, Ordering, metastability and phase transitions in two-dimensional systems, *J. Phys. C* **6**, 1181 (1973).